Absence of Ferroelectric Critical Size in Ultrathin $PbTiO_3$ Nanotubes: A Density-Functional Theory Study

Takahiro Shimada,[1,*] Xiaoyuan Wang,[1] Yoshiaki Kondo,[1] and Takayuki Kitamura[1]

[1]*Department of Mechanical Engineering and Science, Kyoto University, Sakyo-ku, Kyoto 606-8501, Japan*

(Received 16 August 2011; published 10 February 2012)

We simulate from first principles the energetic, structural, and electronic properties of ferroelectric (FE) ultrathin $PbTiO_3$ nanotubes. The nanotube possesses spontaneous polarization despite their sidewalls being thinner than the critical thickness at which the thin films lose ferroelectricity; this indicates the absence of an intrinsic critical size for ferroelectricity. The ground state of the nanotube is not purely FE since it primarily involves antiferrodistortive (AFD) rotations of oxygen atoms due to compression in the inner tube wall. The emergence of the AFD displacement plays a central role in stabilizing both the nanotubular structure and FE distortions due to direct AFD-FE coupling. Moreover, we predict intriguing rich phase transitions due to axial strains including polarization vortices as an important class of nanoscale FE ordering.

DOI: 10.1103/PhysRevLett.108.067601 PACS numbers: 77.80.−e, 31.15.A−, 61.46.Fg

Ferroelectric (FE) perovskite nanotubes have attracted considerable attention as one-dimensional multifunctional nanostructures because of their promising technological applications including nonvolatile FE random access memories and nanoelectromechanical systems [1]. Both the increasing demand to miniaturize such devices and scientific interest in unusual ferroelectricity emerging in the nanoscale components [2] has motivated researchers to synthesize and investigate FE nanotubes. In recent years, various fabrication techniques have been developed [3] and enables us to produce extremely small nanotubes with radii of only 2 nm while preserving both a fine crystalline perovskite structure and chemical stoichiometry [4].

Ferroelectricity in such nanocomponents has attracted great interest. Since ferroelectricity is a collective phenomenon that arises from a delicate balance between long-range Coulomb and short-range covalent interactions, it is very sensitive to the size and shape (ferroelectric-correlation-volume). In addition, a depolarizing field generated by accumulated surface charges, which destabilizes the FE distortion, becomes dominant as materials approach nanoscale dimensions. Thus, there should exist a lower size limit at which ferroelectricity disappears. The critical size for ferroelectricity was first predicted on the basis of classical Landau theory [5]. The critical size has been intensively investigated both experimentally and theoretically, especially, for the thin films: An ultrathin $PbTiO_3$ film epitaxially grown on an insulating $SrTiO_3$ (001) substrate loses ferroelectricity at thicknesses below the two-unit-cell thickness [6]. For ultrathin capacitors in which a FE thin film is sandwiched between two electrodes, the critical thickness still exists to be between two to six unit-cell thicknesses depending on the combination of ferroelectrics and electrode materials used [7–9], due to an inadequate screening effect. However, to the best of the authors' knowledge, the critical size of FE nanotubes has never been reported.

Perovskite oxide nanotubes are subject to internal strain due to the bending moment induced during their construction when rolling up the thin film layers into a tube geometry [10]. Applied strain or stress often affects the FE properties, especially in the nanostructures [11–13]. In fact, the $PbTiO_3$ and $BaTiO_3$ nanotubes exhibit a distinct FE phase transition behavior and higher Curie temperature compared with their counterpart bulk materials [10,14]. This implies that the nature of the FE instability may change in the nanotubes.

The aim of this Letter is to investigate whether ferroelectricity can exist or not in the nanotubes of the prototype ferroelectrics $PbTiO_3$ in which the tube sidewall is thinner than the FE critical thickness of the thin film, using first-principles density-functional theory (DFT) calculations that has successfully predicted the critical thickness of the film and provided microscopic insights into the origin of ferroelectricity at the nanoscale [7–9].

In this Letter, we simulate from first principles within the local density approximation to the density-functional theory using the plane-wave pseudopotential method with plane-wave cutoff energy of 500 eV, as implemented in the VASP code. The electron-ion interaction is described by the projector-augmented wave potentials that explicitly include the Pb $5d$, $6s$, and $6p$, the Ti $3s$, $3p$, $3d$, and $4s$, and the O $2s$ and $2p$ electrons in the valence states. The results presented in this Letter have also been cross-checked using a numerical atomic orbital method as implemented in the SIESTA code, the reliability of which was carefully tested in Ref. [15]. Figure 1 shows the simulation model of a stoichiometric ultrathin $PbTiO_3$ nanotube in which the sidewall has a single-unit-cell-thickness below the critical size of the thin films [6]. The nanotube is modeled by rolling up a (100) ultrathin film about the [001] axis. Thus, the axial, circumferential, radial directions are [001], [010], and [100], respectively. Two possible configurations of the outside-inside tube-wall

 © 2012 American Physical Society

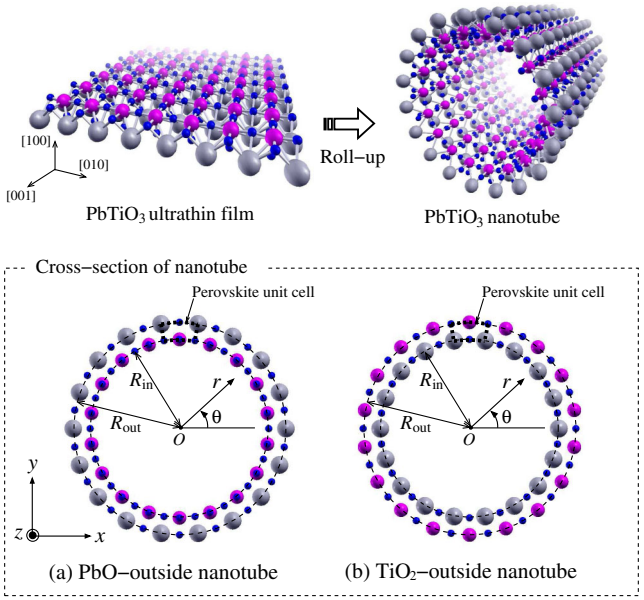

FIG. 1 (color online). Stoichiometric ultrathin $PbTiO_3$ nanotubes. The two possible sidewall configurations of (a) PbO-outside and (b) TiO_2-outside nanotubes are considered.

stacking sequence are considered as the PbO/TiO_2 (PbO-outside) and the TiO_2/PbO (TiO_2-outside) layers [see Figs. 1(a) and 1(b), respectively]. The nanotube radius R is determined by the number of perovskite unit cells N arranged in the circumferential direction. To perform a systematic search for a stable tube configuration, the nanotubes with different radii ($N = 10$–22) are simulated in this study. Within the supercell approach, a 20-Å-thick vacuum layer is introduced in the perpendicular direction to the tube axis. We use a $1 \times 1 \times 6$ Monkhorst-Pack k-point mesh for all of the Brillouin zone integrations. The atomic configurations are fully relaxed until all the forces and stress components are less than 0.01 eV/Å and 0.05 GPa, respectively.

We first calculate the cohesive energy of nanotube, $E_c = (E_{Pb} + E_{Ti} + 3E_O) - E_{tube}/N$, where E_{Pb}, E_{Ti}, and E_O denote the total energy of isolated Pb, Ti, and O atoms, respectively, and E_{tube} is the total energy of the nanotube. Figure 2 shows a plot of the total energy E_{tube} and cohesive energy E_c of the nanotubes as a function of the tube curvature $1/R$, where the radius R is the average of the outside and inside radii, $R = (R_{out} + R_{in})/2$. The cohesive energy is positive (exothermic) for all the nanotubes, which indicates that the nanotube is a stable structure corresponding to a local minimum on the Born-Oppenheimer surface [16,17]. We obtained higher cohesive energies for the PbO-outside nanotubes than that of the flat thin film, which clearly indicates the stability of the nanotubular structure, while the TiO_2-outside case is energetically unfavorable. The highest cohesive energy of $E_c = 39.25$ eV/cell is located at $1/R = 0.089$ Å^{-1} ($N = 18$) for the PbO-outside nanotube in which the outside-PbO and inside-TiO_2 radii are $R_{out} = 11.89$ Å and $R_{in} = 10.17$ Å, respectively. Considering the fact that the flat sheet (thin film with one-unit-cell thickness) has experimentally synthesized and stably exists [6], the PbO-terminated $N = 18$ nanotube, which has a higher cohesive energy by 0.082 eV/cell than that of the flat sheet, can be reasonably more stable. In addition, the cohesive energy of bulk $PbTiO_3$ is $E_c = 40.61$ eV/cell. This value is 1.36 eV/cell (0.272 eV/atom) [18] larger than that of the nanotubes, which indicates that the nanotube is metastable. The similar trend was also found not only in oxide nanotubes (e.g., TiO_2 anatase nanotubes [19]) but also in the metallic nanotubes [16,17,20], which were observed experimentally. For example, the cohesive energy of the experimentally observed (5,3) gold nanotube ($E_c = 2.58$ eV/atom) is smaller than that of the counterpart

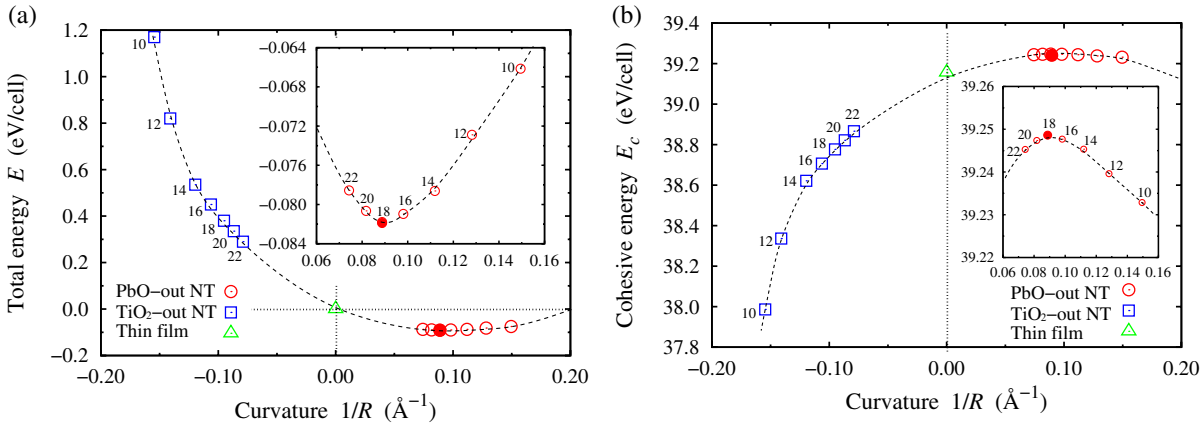

FIG. 2 (color online). (a) Total energy per perovskite unit cell E/N as a function of nanotube curvature $1/R$, where the positive and negative values represent the curvature of the PbO-outside and TiO_2-outside nanotubes (NTs), respectively. The total energy of the flat film is set to zero. The full circle indicate the minimum-energy point. (b) Cohesive energy E_c as a function of nanotube curvature $1/R$. The numbers next to the points denote the number of perovskite unit cells, N.

bulk ($E_c = 3.21$ eV/atom) [16], and the difference is 0.63 eV/atom. This value is larger than that of the $PbTiO_3$ nanotube in the present study, 0.272 eV/atom, which implies that the stability of the $PbTiO_3$ nanotube is relatively higher than the existing metallic nanotubes.

The atomic structure of the minimum-energy $N = 18$ PbO-outside nanotube is shown in Fig. 3. Buckling of the tube sidewall is observed, especially in the inside TiO_2 layer, which is clearly induced by periodic clockwise and counterclockwise tilting of oxygen atoms in the circumferential direction (see the blue triangles and black arrows), namely, the antiferrodistortive (AFD) instability. The AFD rotation of oxygen octahedron TiO_6 is an important class of structural instabilities, but it is generally suppressed in bulk $PbTiO_3$ at equilibrium by FE distortions. However, under high pressures, the AFD instability appears to reduce the strain energy and produce efficient compression of $PbTiO_3$ [21]. Since there is curvature with respect to the flat thin film geometry, bending deformation is homogeneously applied to the tube sidewall. Consequently, the inside TiO_2 layer is subject to relatively high compression. This leads to the emergence of the AFD rotations. In fact, AFD rotations are found in all the PbO-outside nanotubes, whereas AFD rotations are not found in the TiO_2-outside nanotubes in which the TiO_2 layer is subject to tension. Moreover, the emergence of AFD rotation plays a central role in stabilizing the nanotubular structure: When the AFD displacement is artificially excluded in the structural relaxation process by constraining the corresponding degrees of freedom, the total energy of the stable PbO-outside $N = 18$ nanotube dramatically increases above that of flat film. This implies that the structure cannot be stabilized without the AFD rotation because the internal compressive stress in the inside TiO_2 layer can be successfully relaxed by the buckling induced by the AFD displacement [21]. Such buckling of the inside layers and resulting stabilization of the nanotubular structure has also been reported in extremely thin anatase TiO_2 nanotubes [19].

Regarding the ferroelectricity in the PbO outside $N = 18$ nanotube, a nonzero spontaneous polarization is found in the axial z direction of $P_z = 5.12$ μC/cm^2 [22], which is one-order smaller than that of bulk, 78.6 μC/cm^2. On the other hand, the flat thin film is purely paraelectric, which is consistent with an experimentally observed single-unit-cell-thick $PbTiO_3$ film on a $SrTiO_3$ (001) substrate [6]. This indicates that ferroelectricity reappears owing to the nanotubular structure; hence, the nanotubes have no intrinsic critical size. For more detailed discussion, Fig. 4 shows the FE axial polarization P_z and AFD oxygen rotation angle ϕ as functions of the tube curvature $1/R$. Obviously, the FE polarization and AFD rotation are directly coupled to each other: The polarization increases smoothly as the AFD rotation is enhanced by increasing the curvature (compressing the inner TiO_2 layer) for the PbO-outside nanotubes, whereas the TiO_2-outside nanotubes that do not involve any AFD rotation are all paraelectric. In addition, when a constrained relaxation excluding the AFD displacement is performed, all the nanotubes turn back to the paraelectric configuration. This indicates that a purely FE state cannot be stable without AFD distortions. These results suggest that the presence of AFD rotation results in ferroelectricity in the ultrathin $PbTiO_3$ nanotube. A similar FE transition involving the AFD displacement has also been experimentally observed in highly pressurized $PbTiO_3$ [21]: Although polar distortions once disappear at moderate hydrostatic pressures, applying further pressure induces tilting of the AFD oxygen octahedron, leading to the reappearance of the FE state. These results are clearly due to the strong AFD-FE coupling. Recent studies have also reported that the AFD distortion is strongly coupled with electric dipoles, causing anomalous ferroelectricity, e.g., improper phase transitions [23], rich phase diagrams [24], and counterintuitive evolution of the Curie temperature with strain [25]. Considering the fact that the AFD and FE are positively coupled in the presence of "improper"

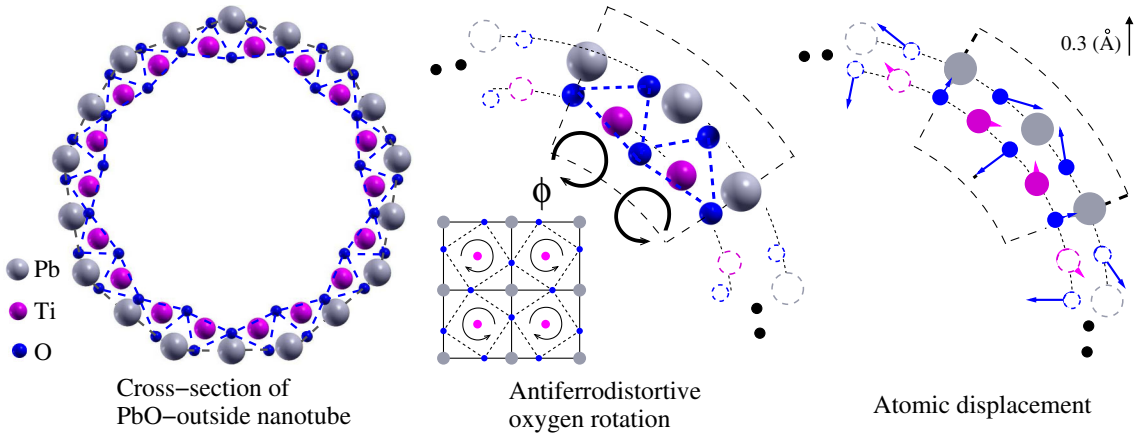

FIG. 3 (color online). Cross section of the stable PbO-outside $N = 18$ nanotube. Antiferrodistortive oxygen rotations ϕ are indicated by the black arrows.

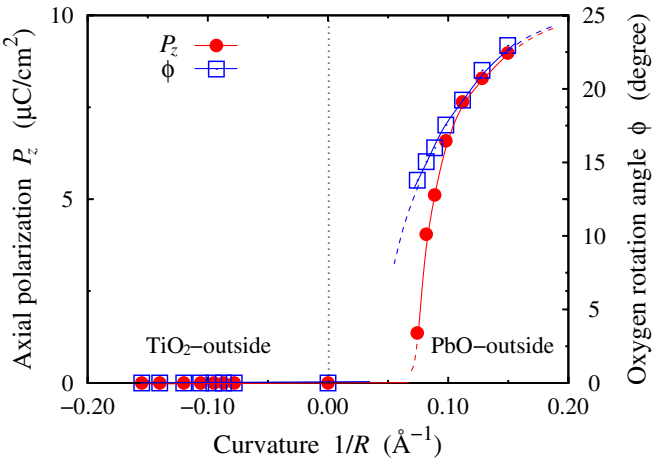

FIG. 4 (color online). Axial ferroelectric polarization P_z and antiferrodistortive oxygen rotation angle ϕ as functions of nanotube curvature $1/R$, where positive and negative values represent the curvatures of the PbO-outside and TiO_2-outside nanotubes (NTs), respectively.

ferroelectricity, e.g., in $PbTiO_3/SrTiO_3$ ultrathin superlattices [23], the nanotube is probably exhibiting the improper ferroelectric transition.

To systematically investigate the effect of axial strain on ferroelectricity in the nanotube, different levels of axial tensile and compressive strains are applied relaxing all the internal degrees of freedom of the atomic coordinates. Figure 5 shows the spontaneous polarization and FE orderings in the stable PbO-outside $N = 18$ nanotube as functions of the axial strain. During tension, FE distortions appear purely in the axial direction (FE_{Axial}) and the axial polarization P_z increases smoothly because the tetragonal distortion of the perovskite lattice increases. The AFD

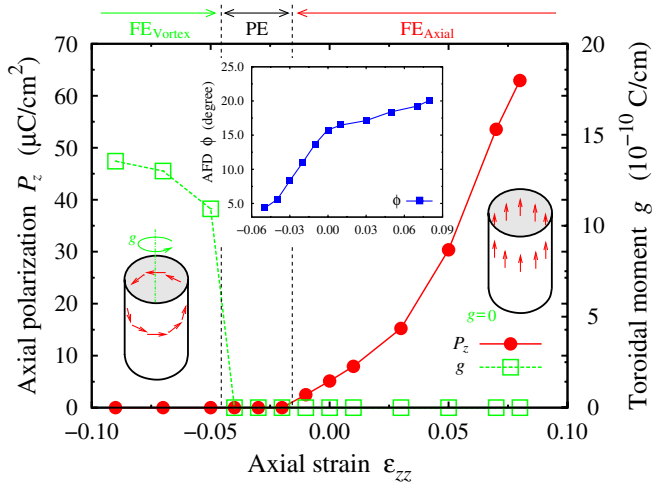

FIG. 5 (color online). Axial polarization, P_z, and toroidal moment, g, of the stable PbO-outside nanotube as functions of axial strain, ε_{zz}. The variation in the AFD rotation angle ϕ with strain is also shown.

oxygen rotation ϕ is enhanced by the application of tensile strain (see the blue lines in Fig. 5), which also supports increase of axial polarization due to direct AFD-FE coupling. On the other hand, under axial compression, the spontaneous polarization disappears at $\varepsilon_{zz} = -0.02$, and the system becomes paraelectric (PE). Further application of compressive strain causes the system to revert the FE phase at $\varepsilon_{zz} = -0.05$. However, a polarization vortex (FE_{Vortex}) forms due to the spontaneous polarization being aligned in the circumferential direction. To evaluate the strength of the polarization vortices, we introduce a toroidal moment g about the tube axis calculated using $g = 1/(2N)\sum \mathbf{r}_i \times \mathbf{P}_i$, where $\mathbf{r}_i$ and $\mathbf{P}_i$ denote the position vector from the tube center and local polarization of the perovskite unit-cell, i, and the sum runs over all the perovskite unit cells in the nanotube. The toroidal moment g, which is also shown in Fig. 5, tends to increase as the compression is applied. Thus, the nanotube exhibits a variety of phase transitions with the application of strain, including the polarization vortex state, which is an important class of FE phases in the nanocomponents.

Finally, we briefly discuss the electronic characteristics of the nanotubes. The stable PbO-outside nanotube exhibits a wider band gap energy of $E_g^{Tube} = 2.21$ eV than that of the bulk $E_g^{Bulk} = 1.65$ eV. This suggests that the ultrathin nanotube possesses strong resistance to electric current leakage, which is often the case with FE nanodevices. Such a relatively wide band gap energy has also been found in ultrathin anatase TiO_2 nanotubes [19]. The band gap energy in the nanotube is found to be sensitive to the strain: E_g changes from 2.90 to 1.91 eV with the axial strain range from $\varepsilon_{zz} = 0.10$ to -0.10. In contrast, the change in band gap energy in the bulk is relatively small, being less than 0.3 eV in the same strain range. Note that, although these band gap energies are less than the experimentally measured value (e.g., $E_g^{Bulk} = 3.5$ eV for bulk) [26] owing to the well-known problem within the framework of standard DFT, the result should be qualitatively correct.

In summary, our DFT calculations provide insightful results on the structural, ferroelectric, and electronic properties of ultrathin $PbTiO_3$ nanotubes. Ferroelectricity can be retained in the nanotube with the sidewalls thinner than the critical limit of the thin film geometry, which indicates the absence of a critical size. This is because the antiferrodistortive oxygen rotation induced by the nanotubular shape involves ferroelectric distortions. The calculations also predict intriguing rich phase transitions by strain including a ferroelectric vortex and a wide band gap energy, which should be promising for ferroelectric nanodevices.

The authors acknowledge financial support for T. S. and T. K. from the Grant-in-Aid for Scientific Research (S) (Grant No. 21226005) and the Grant-in-Aid for Young Scientists (A) (Grant No. 23686023) of the Japan Society of the Promotion of Science (JSPS).

*shimada@cyber.kues.kyoto-u.ac.jp

[1] R. Ramesh, *Thin Film Ferroelectric Materials and Devices* (Kluwer Academic Publishers, Boston, 1997).

[2] I. I. Naumov, L. Bellaiche, and H. Fu, Nature (London) **432**, 737 (2004).

[3] X. Zhu, Z. Liu, and N. Ming, J. Mater. Chem. **20**, 4015 (2010).

[4] Y. Mao, S. Banerjee, and S. S. Wong, Chem. Commun. (Cambridge) **3**, 408 (2003).

[5] R. Kretschmer and K. Binder, Phys. Rev. B **20**, 1065 (1979).

[6] D. D. Fong, G. B. Stephenson, S. K. Streiffer, J. A. Eastman, O. Auciello, P. H. Fuoss, and C. Thompson, Science **304**, 1650 (2004).

[7] J. Junquera and P. Ghosez, Nature (London) **422**, 506 (2003).

[8] N. Sai, A. M. Kolpak, and A. M. Rappe, Phys. Rev. B **72**, 020101(R) (2005).

[9] Y. Umeno, B. Meyer, C. Elsässer, and P. Gumbsch, Phys. Rev. B **74**, 060101(R) (2006).

[10] Y. Yang, X. Wang, C. Sun, and L. Li, J. Appl. Phys. **104**, 124108 (2008).

[11] T. Shimada, S. Tomoda, and T. Kitamura, Phys. Rev. B **79**, 024102 (2009).

[12] T. Shimada, S. Tomoda, and T. Kitamura, J. Phys. Condens. Matter **22**, 355901 (2010).

[13] Y. Umeno, T. Shimada, T. Kitamura, and C. Elsässer, Phys. Rev. B **74**, 174111 (2006).

[14] Y. Yang, X. Wang, C. Sun, and L. Li, J. Appl. Phys. **109**, 014109 (2011).

[15] T. Shimada, X. Wang, S. Tomoda, P. Marton, C. Elsässer, and T. Kitamura, Phys. Rev. B **83**, 094121 (2011).

[16] R. T. Senger, S. Dag, and S. Ciraci, Phys. Rev. Lett. **93**, 196807 (2004).

[17] T. Shimada, Y. Ishii, and T. Kitamura, Phys. Rev. B **84**, 165452 (2011).

[18] This value is obtained by the VASP code. The SIESTA code gives a slightly higher value of 1.48 eV/cell (0.296 eV/atom).

[19] A. M. Ferrari, D. Sziberth, and Y. Noel, J. Mater. Chem. **21**, 4568 (2011).

[20] S. L. Elizondo and J. W. Mintmire, Phys. Rev. B **73**, 045431 (2006).

[21] P. E. Janolin, P. Bouvier, J. Kreisel, P. A. Thomas, I. A. Kornev, L. Bellaiche, W. Crichton, M. Hanfland, and B. Dkhil, Phys. Rev. Lett. **101**, 237601 (2008).

[22] Polarization is calculated via $\mathbf{P} = (1/\Omega)\sum \mathbf{Z} \cdot \mathbf{u}$, where Ω, $\mathbf{Z}$, and $\mathbf{u}$ denote the volume of the cell, Born effective charge tensor, and atomic displacement, respectively. The reference structure for the displacement is taken from the relaxed paraelectric structure.

[23] E. Bousquet, M. Dawber, N. Stucki, C. Lichtensteiger, P. Hermet, S. Gariglio, J. M. Triscone, and P. Ghosez, Nature (London) **452**, 732 (2008).

[24] I. A. Kornev, L. Bellaiche, P. E. Janolin, B. Dkhil, and E. Suard, Phys. Rev. Lett. **97**, 157601 (2006).

[25] D. Sichuga, I. Ponomareva, and L. Bellaiche, Phys. Rev. B **80**, 134116 (2009).

[26] J. Robertson and C. W. Chen, Appl. Phys. Lett. **74**, 1168 (1999).